Pattern Spectrum and Multiscale Shape Representation

PETROS MARAGOS, MEMBER, IEEE

Abstract—**This paper reports the results of a study of multiscale shape description, smoothing and representation. Multiscale nonlinear smoothing filters are first developed by using morphological openings and closings. These filters smooth signals while preserving their edges, and use a definition of scale that agrees with the spatial size of image objects. Matheron used openings and closings to obtain probabilistic size distributions of Euclidean-space sets (continuous binary images). We view these distributions as a concept of pattern spectrum (a shape-size descriptor). Then we develop a pattern spectrum for continuous graytone images and arbitrary multilevel signals, as well as for discrete images by using a discrete-size family of patterns. The pattern spectrum quantifies various aspects of the shape-size content of a signal. Large impulses in the pattern spectrum at a certain scale indicate the existence of major (protruding or intruding) substructures of the signal at that scale. An entropy-like shape-size complexity measure is also developed based on the pattern spectrum. For shape representation, a reduced morphological skeleton transform is introduced for discrete binary and graytone images. This transform is a sequence of skeleton components (sparse images) which represent the original shape at various scales. It is shown that the partially reconstructed images from the inverse transform on subsequences of skeleton components are the openings of the image at a scale determined by the number of eliminated components; in addition, two-way correspondences are established among the degree of shape smoothing via multiscale openings or closings, the pattern spectrum zero values, and the elimination or nonexistence of skeleton components at certain scales. All the above results provide useful tools for multiscale shape representation and description.**

Index Terms—**Mathematical morphology, multiscale image analysis, nonlinear smoothing, shape description, shape representation, skeletonization.**

I. Introduction

THE problem of shape representation and shape-size description is very important in computer vision and image processing. Toward this goal, this paper develops a shape-size descriptor, called *pattern spectrum*, which can detect critical scales in an image object and quantify various aspects of its shape-size content, as well as a related multiscale shape representation scheme based on *skeleton transforms*. The unifying theme in both of these areas is the repeated use of families of *multiscale nonlinear smoothing* filters. Next, we provide a qualitative discussion of the ideas presented in this paper.

Manuscript received September 26, 1987; revised March 29, 1988. This work was supported by the National Science Foundation under Grant CDR-85-00108, and by a National Science Foundation PYIA under Grant MIPS-86-58150 with matching funds from Bellcore, Xerox, and an IBM Departmental Grant.

The author is with the Division of Applied Sciences, Harvard University, Cambridge, MA 02138.

IEEE Log Number 8928049.

By *shape* is meant any image conveying information about intensity or range, or any other finite-extent signal whose graph is viewed as an image object conveying some pictorial information. By *scale* we define here the *smallest size* of a shape pattern (generated by a prototype pattern of unit size) that can fit inside the image. Recently, the necessity of multiscale[1] image analysis has been recognized in various tasks of computer vision [1]–[4]. Scale in all these approaches has been quantified by linearly convolving the image with a Gaussian function of standard deviation σ or with local weighted averagers of spatial span $\sigma \geq 0$; the real number σ is the scale parameter. This linear filtering approach to multiscale image analysis has gained popularity because of its mathematical tractability, its close relationships with Fourier analysis, and its plausibility for being used at the early stages of the human visual system. However, we also see three rather weak points: 1) *linear* filters shift and blur important image features such as edges, 2) their implied scale parameter (average width of their impulse response) is not directly related to our aforementioned size-based definition of scale, and 3) the multiscale filtered versions of the signal do not correspond to a compact shape representation, except for the obvious one, that is, the difference signals between filtered versions at successive scales. Alternatively, there is a large class of *nonlinear* filters that avoid some or all of the three aforementioned problems. They include *median* filters and *opening/closing* filters [6]–[12]. Matheron [6], [47] used openings of sets in Euclidean spaces by compact convex sets of varying size (scale) to axiomatize the concept of size. Openings of 1D boundaries of continuous binary images by disks of varying radius (scale) were used in [15] to obtain results for scale-space zero-crossing maps similar to [2], [3]. A multiresolution approach based on openings/closings was also developed in [16]. Both median and opening/closing filters can be defined based on a scale parameter and provide signal smoothing by eliminating impulses (whose spatial width is smaller than the filter's scale) while preserving its edges. In this paper, we deal only with openings/closings, because they are directly related [12] to a well-known shape representation, i.e., the *medial axis transform* (MAT), and we will use them to develop a shape-size descriptor, the pattern spectrum, explained next.

[1]This paper does *not* deal with *multiresolution* image analysis, which involves both multiscale image filtering and subsampling the image at coarser scales; multiresolution approaches can be found in [5].

A measure of the *spectral content* of a signal $s(t)$ in a certain frequency ω can be obtained from multiplying $s(t)$ with the complex sinusoid $e^{-i\omega t}$ and measuring the area under the modulated signal $s(t)e^{-i\omega t}$. By varying the frequency ω a *frequency spectrum* of the signal is obtained, which is the well known Fourier transform. From an abstract viewpoint, we can view $e^{-i\omega t}$ as a probing *pattern* that interacts with the original signal $s(t)$ and extracts some information (spectral content) from it by *transforming* it first via modulation and then by performing a *measurement* on the transformed signal. The probing pattern $e^{-i\omega t}$ is a signal depending on a single *frequency parameter* ω, and its own Fourier spectrum is an impulse at frequency ω. Despite the monumental significance and usefulness of the Fourier spectrum in the evolution of signal and image processing, it has little to offer in quantifying the *shape and size content* of signals (such as images) possessing geometrical structure. However, the aforementioned abstract concepts that are implicitly used to obtain the Fourier spectrum are of general importance, and we use them in this paper to develop a *pattern spectrum* for images and signals, reporting earlier work in [12]–[14] on this subject. To give the reader an intuitive feeling of these ideas, we outline our approach for binary images. Thus we replace the function representing the signal $s(t)$ with a 2D set X representing a binary image; the complex sinusoid with a compact 2D set B_n depending on a size (scale) parameter n; the signal modulation with a shape-size transformation of X. Then we use the area of the transformed image to obtain a pattern spectrum of X that measures the size distribution in X relative to the shape of B_n. The shape-size transformations of X by B_n are morphological openings. Such openings of continuous-space sets (binary images) by one-parameter families of compact convex sets were developed by Matheron [6], [47] (who called them *granulometries*) to unify all sizing (sieving) set operations in Euclidean spaces; Lebesgue measures of the openings were then used to define probabilistic size distributions that form part of his theory for random sets. As described in [7, ch. 10], Serra and his co-workers have used extensively these size distributions in image analysis applications to petrography and biology. In this paper we view these size distributions via the concept of a pattern spectrum. We also extend the size distributions and pattern spectrum to continuous-space graytone images and arbitrary multilevel signals, as well as to discrete-space binary and graytone images by introducing a discrete-size family of patterns. All the aforementioned ideas are then related to the MAT.

The MAT, also called the skeleton transform or the symmetric axis transform, since its first introduction by Blum [17], [18] has received much attention for 2D or 3D shape description [19], [20]. It is one of the major *information preserving* algorithms for shape analysis [21] and is closely related to the smoothed local symmetries [22] or to other axial shape representations [23]. The MAT is the set of the centers of the maximal disks (spheres) inscribable inside the 2D (3D) image object. It can be found via a well-known wavefront propagation. This propagation can be modeled either via the *distance* transform approach [24]–[25], or via iterated *shrink/expand* operations for binary images [26] which become *min/max* operations for graytone images [27]–[29]. Such shrink/expand image operations and other related Boolean-type signal convolutions [30], [31] have been used extensively in cellular array computers for image processing. All shrink/expand and min/max image operations can be formalized and further extended by a large class of nonlinear filters called *morphological filters* [6]–[12], which include the erosion (shrink), dilation (expand), opening (cascade of shrink-expand), and closing (cascade of expand-shrink). In [12], [10], [11] a unified theory has been developed which shows that a large class of nonlinear and linear image processing systems can be represented as a minimal superposition of erosions or dilations. Consequently, among the numerous approaches to find the MAT,[2] it can also be obtained via erosions and openings [33], [7], [34]; we refer to this last approach as the *morphological skeleton transform*. The morphological approach to skeletonization is formal, avoids ad hoc algorithms, and has some other advantages [34]. In this paper, we modify the morphological skeleton transform to develop a *reduced skeleton transform* (RST). By "reduced" is meant that some (but not all) redundancy is taken out of the skeleton while preserving its ability for exact image reconstruction. The RST is a collection of skeleton components (sparse images) that represent the original shape at various scales. In general, by eliminating components (bones) of the original or reduced skeleton transform, we reconstruct (from the pruned skeleton) smoother versions of the original shape; these smoother versions are its openings at successive scales. Thus, we achieve a multiscale shape representation which is in a one-to-one correspondence with a multiscale nonlinear shape smoothing. The reason for using *reduced* skeleton components is because of their direct relation to the pattern spectrum. That is, we show in this paper that eliminating any reduced skeleton component is equivalent to zeroing the value of the pattern spectrum at the corresponding scale.

This paper is organized as follows. In Section II, we develop multiscale nonlinear smoothing filters (openings and closings) that depend on a structuring pattern and on a scale parameter. For continuous-space binary signals, the scale is based on a concept of size quantified via positive homothetics; for multilevel signals we generalize this by using set-theoretic representations of signals. For discrete-space signals we introduce a definition of scale based on dilations. By using the continuous multiscale filters of Section II, Section III defines the pattern spectrum for continuous-space binary images and extends it to graytone images or arbitrary signals. The discrete multiscale filters of Section II are used in Section IV to develop a pattern spectrum for discrete-space images. Section V de-

[2]There is a voluminous literature on skeletonization algorithms, most of which can be defined via shrink/expand operations. Many of these algorithms, e.g., [32], emphasize the *connectivity* of the skeleton, which is of no concern to us in this paper.

fines an *oriented* pattern spectrum, which is able to extract information about 1D structures located in 2D space. In Section VI, an "entropy-like" shape-size complexity measure is introduced based on the pattern spectrum. The multiscale shape representation based on RST is developed in Section VII for binary images and in Section VIII for graytone images; these sections also relate the RST to the pattern spectrum and the multiscale nonlinear smoothing. In Section IX, we conclude and outline some possible applications of the pattern spectrum and the RST.

II. Multiscale Nonlinear Smoothing

A. A Definition of Size (Scale)

1) Continuous Size: Let $\boldsymbol{R}$ and $\boldsymbol{Z}$ denote, respectively, the set of real numbers and integers. Let B be a compact connected subset of the plane $\boldsymbol{R}^2$; we call such B a *continuous-space binary pattern*. If B has size (by convention) one, then the set

$$rB = \{rb: b \in B\}, \qquad r \geq 0, \tag{1}$$

defines a pattern of *continuous size* r where r is any nonnegative real number. The pattern rB has the same shape as B.

Let $g(x, y)$ be a 2D real-valued function whose support is a compact connected subset of $\boldsymbol{R}^2$. Its *umbra* [8] is the set

$$U(g) = \{(x, y, a) \in \boldsymbol{R}^3: g(x, y) \geq a\}. \tag{2}$$

From $U(g)$ we can reconstruct g since

$$g(x, y) = \sup\{a \in \boldsymbol{R}: (x, y, a) \in U(g)\}. \tag{3}$$

If we view g as a *graytone pattern* of size one, then we define as a pattern of continuous size $r \geq 0$ the function

$$(rg)(x, y) = \sup\{a \in \boldsymbol{R}: (x, y, a) \in rU(g)\} \tag{4}$$

where $rU(g)$ is obtained from (1). That is, $U(rg) = rU(g)$. The function rg has the same shape as g, but both its support and range will be scaled by a factor r.

2) Discrete Size: Both (1) and (4) are not useful for defining the size of discrete patterns. For example, Fig. 1 shows that, if B is a 2D discrete square of size one, then the definition $2B$ via (1) gives not a square of size 2 but the corner points of such a square. This led us to give an alternative definition of discrete size based on set dilation. If X, Y are subsets of $\boldsymbol{R}^m$ or $\boldsymbol{Z}^m$, the *dilation* (also known as Minkowski sum [35]) of X and Y is the set

$$X \oplus Y = \{a + b: a \in X, b \in Y\} = \bigcup_{p \in Y} X + p \tag{5}$$

where $X + p = \{a + p: a \in X\}$ denotes the *translate* of X by the vector p. (Note that, if $a = (a_1, a_2)$, $b = (b_1, b_2) \in \boldsymbol{R}^2$ and $r \in \boldsymbol{R}$, we use the notation $a \pm b = (a_1 \pm b_1, a_2 \pm b_2)$ and $rb = (rb_1, rb_2)$.) Let B be a *discrete-space binary pattern*, that is, a finite connected subset of the discrete plane $\boldsymbol{Z}^2$. If B is of size (by convention) one, then the finite sets

$$nB = \underbrace{B \oplus B \oplus \cdots \oplus B}_{n \text{ times}} \tag{6}$$

define a family of binary patterns generated by B and parameterized by the *discrete size parameter* $n = 0, 1, 2, \cdots$. If $n = 0$, $nB = \{(0, 0)\}$ by convention. Note that $nB \oplus mB = (n + m)B$ for any set B and for any nonnegative integers m, n. If B is convex, then nB is shaped like B but has size n, as Fig. 1 shows. The shape of nB is controlled by the shape of the primary pattern B, whereas n controls the size. This concept of discrete shape-size family of patterns was used in [12], [34] for morphological skeletonization.

Similarly, let $g(x, y)$ be a *discrete-space graytone pattern*, that is, a real-valued function whose support is a finite connected subset of $\boldsymbol{Z}^2$, of size one. If

$$(f \oplus g)(x, y) = \max_{(i,j)} \{f(x - i, y - j) + g(i, j)\} \tag{7}$$

denotes the *dilation* [8] of some function f and g, the function

$$ng = \underbrace{g \oplus g \oplus \cdots \oplus g}_{n \text{ times}} \tag{8}$$

defines a function pattern of discrete size $n = 0, 1, 2, \cdots$. Note that our definition of size in (1), (4), (6), and (8) is independent of the area of the size-one pattern B or g.

The definitions (1) and (6) of continuous and discrete size are compatible when $B \subseteq \boldsymbol{R}^2$ is *convex* [6] because then $2B = \{2b: b \in B\} = B \oplus B$. Hence, the set dilation can provide us with a discrete-size family of convex patterns B, which are identical to those obtained via the positive homothetics rB of (1) for r evaluated at integer values. Similar ideas apply for a continuous graytone pattern g whose umbra is convex because then the definitions (4) and (8) are compatible for integer r. Examples of patterns nB and ng are shown in Fig. 2.

B. Filters for Binary Images

For sets X, Y in $\boldsymbol{R}^m$ or $\boldsymbol{Z}^m$, the *opening* [35], [6] of X by Y is the set $X \circ Y = (X \ominus Y) \oplus Y$, where

$$X \ominus Y = \{a: Y + a \subseteq X\} = \bigcup_{p \in Y} X - p \tag{9}$$

is the *erosion* [35], [7] of Y from X. The set $X \bullet Y = (X \oplus Y) \ominus Y$ is called[3] the *closing* [6] of X by Y.

We henceforth denote a discrete-space *binary image* by a *set* X in $\boldsymbol{Z}^2$; the set complement X^c denotes the image background. Let $B \subseteq \boldsymbol{Z}^2$ be a fixed pattern. (In the context of morphology B is called a set *structuring element* [7].) We define as a *multiscale opening* of X by B at scale

[3]In the recent literature on morphology, there are mainly two slightly different sets of definitions: one of [6], [7], and another of [8], [9]. Maragos and Schafer used in [10]–[14] and [34], [36] the definitions from Matheron and Serra. In this paper, we follow the definitions of Sternberg, Haralick *et al.* because they are simpler. Our only difference is to use the group-theoretic notation $S + x$ for set translation. Note also that Hadwiger [35] originally called Minkowski sum and difference what we call here dilation and erosion.

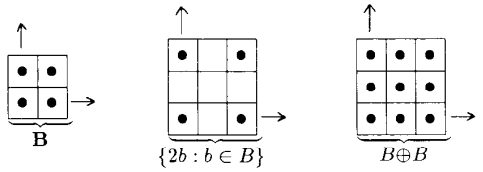

Fig. 1. Two definitions of discrete size. (Pixels with a • denote points in the image (set) X; empty pixels are points in the complement X^c.)

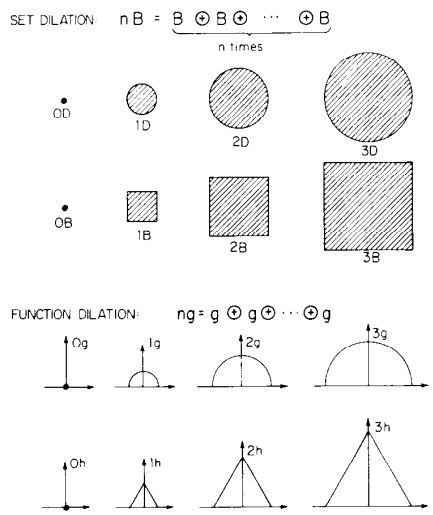

Fig. 2. Discrete-size families of binary and graytone patterns.

$n = 0, 1, 2, \cdots$, the opening

$$X \circ nB = (X \ominus nB) \oplus nB \tag{10}$$

of X by nB. A *dual* (with respect to complementation) multiscale filter is the closing of X by nB:

$$X \bullet nB = (X \oplus nB) \ominus nB = (X^c \circ n\check{B})^c \tag{11}$$

where $\check{B} = \{-b: b \in B\}$ is the *reflected* (symmetric) set of B. If $n = 0$, then $X \circ nB = X \bullet nB = X$. For any sets A, B, C, $(A \ominus B) \ominus C = A \ominus (B \oplus C)$ and $(A \oplus B) \oplus C = A \oplus (B \oplus C)$; hence, (10) can be implemented more efficiently as

$$X \circ nB = \underbrace{[(X \ominus B) \ominus B \cdots \ominus B]}_{n \text{ times}} \underbrace{\oplus B \oplus B \cdots \oplus B}_{n \text{ times}} \tag{12}$$

Likewise for $X \bullet nB$. The implementation (12) has *linear* complexity with respect to the number of points in B, whereas (10) has *quadratic* complexity [34]. If B has a regular shape, then $X \circ nB$ and $X \bullet nB$ provide multiscale nonlinear smoothing of the boundary of X, but they are region-based image operations. Fig. 3 shows the multiscale opening and closing of a binary image X by a pattern B, which is the octagon of Fig. 4. The opening suppresses the sharp capes and cuts the narrow (relative to nB) isthmuses of X. The closing $X \bullet nB$ provides a multi-scale nonlinear smoothing of the background of X. That is, the closing fills in the gulfs and the small (relative to nB) holes of X.

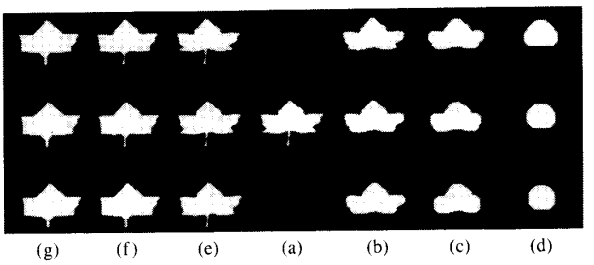

Fig. 3. Multiscale *SP* openings and closings. (a) Discrete binary image X of 85 × 128 pixels. (b) $X \circ nB$, $n = 1, 2, 3$ (top to bottom) where B is the octagon of Fig. 4. (c) $X \circ nB$, $n = 4, 5, 6$ (top to bottom). (d) $X \circ nB$, $n = 7, 8, 9$ (top to bottom). (e) $X \bullet nB$, $n = 1, 2, 3$ (top to bottom). (f) $X \bullet nB$, $n = 4, 5, 6$ (top to bottom). (g) $X \bullet nB$, $n = 7, 8, 9$ (top to bottom).

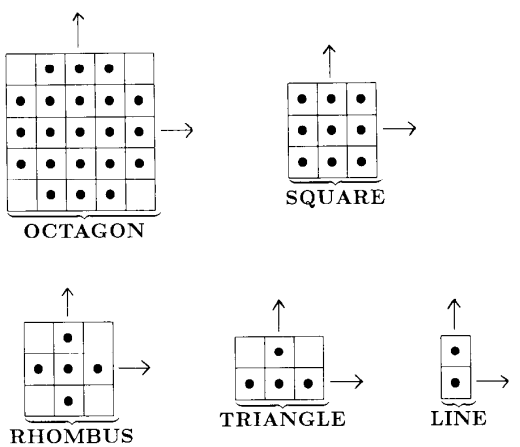

Fig. 4. Binary patterns in $\mathbf{Z}^2$.

From (10), (5) and (9) it follows that

$$X \circ nB = \bigcup_{nB + z \subseteq X} (nB) + z. \tag{13}$$

Hence, $X \circ nB$ eliminates from X all objects of size $< n$ (with respect to B), that is, objects inside which nB cannot fit. That is why, we use the size n of nB as synonymous to the scale at which the filter $X \circ nB$ operates.

C. Filters for Graytone Images

Following the terminology of [10], we call (10) and (11) *set-processing* (SP) opening/closing because both their inputs and outputs are sets (binary images). Similarly, we henceforth represent *graytone images* by *functions*; filters whose inputs and outputs are functions (multilevel signals) are called *function-processing* (FP) filters. Let $f(x, y)$ be a finite-support graytone image function on $\mathbf{Z}^2$, and let $g(x, y)$ be a fixed graytone pattern of size one. (In the context of morphology, g is called a function structuring element [7].) The *erosion* [8] of f by g is the

may also be smaller than the dimensionality of the signal X or f.

III. Pattern Spectrum of Continuous-Space Images

Consider a compact binary image $X \subseteq \boldsymbol{R}^2$ and disks rD of radius r. The *area* of the opening of X by each disk rD, normalized by the area $A(X)$ of X, creates the monotonic decreasing function $F(r) = A(X \circ rD)/A(X)$, $r \geq 0$, which is continuous from the left. In [6], [7] the function $1 - F(r)$ was related to probabilistic measures of the size distribution in X, either itself as a cumulative distribution function, or its derivative as a probability density function. It was also extended to negative values of r by considering the closings of X by rD. The disk D can be replaced by any *compact convex* set in $\boldsymbol{R}^2$. Discrete versions were used in [7, pp. 336–344] for hexagonally-sampled images by replacing the disks with discrete hexagons. In this section we view these size distributions as a concept of a pattern spectrum for continuous-space binary images. Then we extend them by formally defining a pattern spectrum for continuous-space graytone images and arbitrary multilevel signals.

A. Binary Images

We define the *pattern spectrum* of a compact binary image $X \subseteq \boldsymbol{R}^2$ relative to a *convex* binary pattern $B \subseteq \boldsymbol{R}^2$ as the (differential size distribution) function

$$PS_X(r, B) = \frac{-dA(X \circ rB)}{dr}, \qquad r \geq 0. \tag{22}$$

The size parameter r defines the scale. The rationale behind our term "pattern spectrum" is the fact that [see also (13)] the opening $X \circ rB$ is the union of all $rB + z$ with $rB + z \subseteq X$, that is, of all the patterns shaped like B of size r (located at points z) that can fit inside X. Thus, $A(X \circ rB)$ is a measure of the pattern content of X relative to the pattern rB. By varying both r and the shape of B we obtain a *shape-size spectrum* of X, which is the full pattern spectrum of X relative to all the patterns that can fit inside X. By keeping B fixed, (22) becomes a *size histogram* of X relative to B. If any of X or B is fixed, we will suppress it from the general notation of (22). By using closings, (22) can be extended to "negative" sizes r, i.e.,

$$PS_X(-r, B) = \frac{dA(X \bullet rB)}{dr}, \qquad r > 0. \tag{23}$$

Convexity of B guarantees nonnegativity of the pattern spectrum for all $r \in \boldsymbol{R}$ because $X \circ rB \supseteq X \circ sB$ if $r < s$ [6].

Since X is compact, there is a maximum positive size p such that $X \circ rB = \varnothing$ for all $r > p$. Thus, the pattern spectrum will contain at least one Dirac impulse (at $r = p$). In addition, if $CH(X)$ denotes the *convex hull* of X, that is, the smallest convex set containing X, then $X \bullet rB \subseteq X \bullet sB \subseteq CH(X)$ for all $s > r \geq 0$ [6, p. 21]. Hence, there is a size $c > 0$ such that $X \bullet cB = \mathcal{C} = \lim_{r \to \infty} X \bullet rB$. Obviously, $\mathcal{C} \subseteq CH(X)$ and $PS(-r) = 0$ for all $r > c$. If B has a nonempty interior and admits a finite curvature at each point of its boundary (e.g., if B is a disk), then $\mathcal{C} = CH(X)$ [6], [7, p. 100]. Fig. 7 shows $PS_X(r)$ (B is a disk) for X being a disk, circle, and a disk with a hole; their pattern spectra are reminiscent of Fourier transforms of $e^{i\omega_0 t}$, $e^{-i\omega_0 t}$, and $\cos \omega_0 t$, respectively. Additional examples of pattern spectra are shown in Fig. 8; there we see that reconstruction of an image from the pattern spectrum may not be generally possible because there may exist two different images with similar pattern spectra.

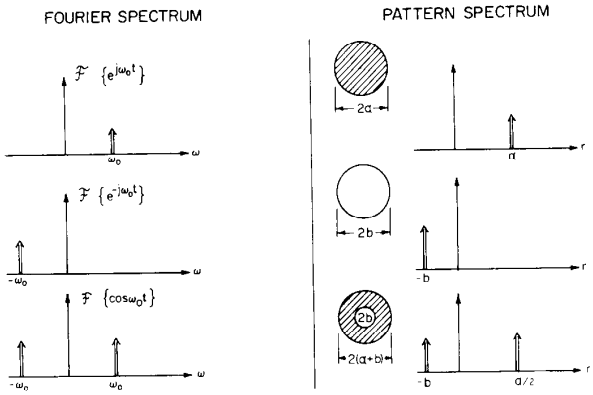

Fig. 7. Conceptual analogies between Fourier spectrum and pattern spectrum.

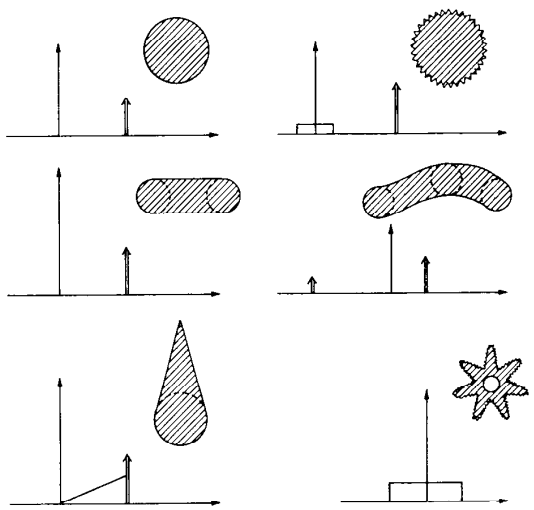

Fig. 8. Pattern spectra of binary images relative to a disk. (The hand-drawings are only qualitative, and some examples are adapted from Serra [7, p. 337].)

The pattern spectrum conveys four (among others) useful types of information about X. First, the *boundary roughness* of X relative to B manifests itself as contributions in the lower size part of the pattern spectrum. Second, the existence of long capes or bulky protruding parts in X that consist of patterns sB shows up as isolated impulses in the pattern spectrum around positive $r = s$. Third, the B-shapiness of X, that is, the maximal degree that X contains the pattern B (or that X contains

function

$$(f \ominus g)(x, y) = \min_{(i,j)} \{ f(x + i, y + j) - g(i, j) \}. \quad (14)$$

Then the opening and closing [8] of f by g are, respectively, the functions $f \circ g = (f \ominus g) \oplus g$ and $f \bullet g = (f \oplus g) \ominus g$. To implement (7) and (14) we assume that f and g are equal to $-\infty$ outside their supports where $\mathrm{Spt}(f) = \{x : f(x) \neq -\infty\}$ denotes the *support* of f. Thus, essentially, these max-of-sums and min-of-differences operations take place only over the moving finite support of g. A more detailed discussion of the definitions and properties of graytone image erosions, dilations, openings, and closings can be found in [7]–[12].

We define the function

$$f \circ ng = (f \ominus ng) \oplus ng \quad (15)$$

as the *multiscale FP opening* of f by g at scale $n = 0, 1, 2, \cdots$. Likewise, the function

$$f \bullet ng = (f \oplus ng) \ominus ng \quad (16)$$

is the *multiscale FP closing* of f by g. As in (12), we can implement (15) more efficiently as

$$f \circ ng = [\underbrace{(f \ominus g) \ominus g \cdots \ominus g}_{n \text{ times}}] \underbrace{\oplus g \oplus g \cdots \oplus g}_{n \text{ times}} \quad (17)$$

Likewise for $f \bullet ng$. Examples of multiscale opening/closing of a graytone image by a graytone pattern g (the upper half of a discrete approximation to a sphere) are shown in Fig. 5.

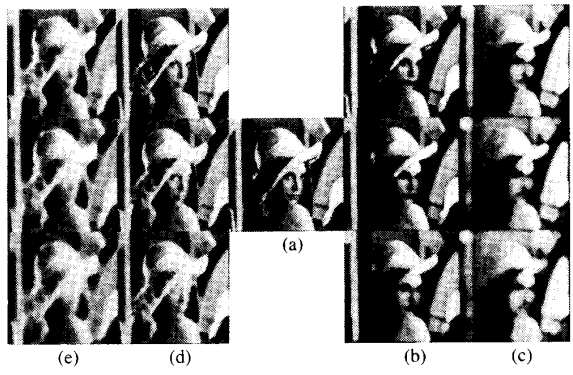

Fig. 5. Multiscale *FP* openings and closings. (a) Graytone image f (256 × 256 pixels). (b) $f \circ ng$, $n = 1, 2, 3$ (top to bottom). The pattern g is defined on $\mathbf{Z}^2$ as $g(x, y) = 5\sqrt{5 - x^2 - y^2}$, $0 \leq x^2 + y^2 \leq 5$, and $g(x, y) = -\infty$ if $x^2 + y^2 > 5$. (c) $f \circ ng$, $n = 4, 5, 6$ (top to bottom). (d) $f \bullet ng$, $n = 1, 2, 3$ (top to bottom). (e) $f \bullet ng$, $n = 4, 5, 6$ (top to bottom).

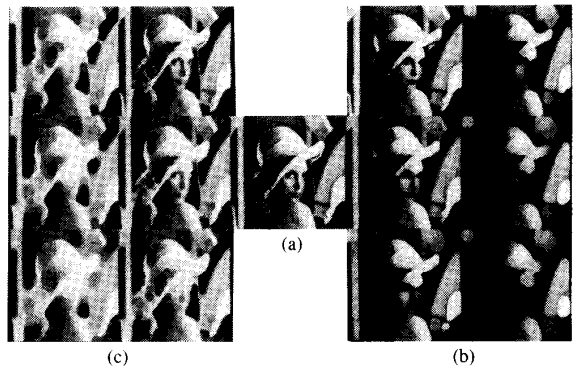

Fig. 6. Multiscale *FSP* openings and closings. (a) Graytone image f of Fig. 5(a). (b) $f \circ nB$, $1 \leq n \leq 6$ where B is the octagon of Fig. 4. (c) $f \bullet nB$, $1 \leq n \leq 6$. The twelve filtered images have been arranged by the size n exactly as in Figs. 5(b)–(e).

D. Filters for Graytone and Binary Images

Referring to Section II-C, if g is binary function equal to 0 inside its support and $-\infty$ elsewhere, then $f \oplus g$ and $f \ominus g$ become, respectively,

$$(f \oplus B)(x, y) = \max_{(i,j) \in B} \{ f(x - i, y - j) \} \quad (18)$$

$$(f \ominus B)(x, y) = \min_{(i,j) \in B} \{ f(x + i, y + j) \} \quad (19)$$

where $B = \mathrm{Spt}(g)$ is a binary pattern. That is, $f \oplus B$ and $f \ominus B$ are the moving local max and min image operations investigated in [27], [29]. If f is binary, then $f \oplus B$ and $f \ominus B$ yield binary images (sets). Hence, we call such operations *function- and set-processing (FSP)*. Further, we define the functions

$$f \circ nB = (f \ominus nB) \oplus nB, \quad (20)$$

$$f \bullet nB = (f \oplus nB) \ominus nB, \quad (21)$$

respectively, as the *multiscale* FSP *opening* and *closing* of f by B at scale $n = 0, 1, 2, \cdots$. Obviously, FSP multiscale opening/closing are special cases of their FP counterparts. Meyer [45] used closings by hexagons of increasing sizes in analyzing digital graytone biomedical images. Examples of FSP opening and closing of a graytone image by a binary pattern B at multiple scales are shown in Fig. 6. The nonlinear smoothing effects of the multiscale opening/closing by B are very comparable to the similar smoothing by g in Fig. 5 because B and g had the same (21 pixel) support. However, at large scales n the opening $f \circ nB$ creates some large flat plateaus shaped like nB; likewise, the closing $f \bullet nB$ creates large flat sinks shaped liked nB. By contrast, the multiscale opening (closing) by g will give these summits (sinks) a form of peaks (valleys) shaped like ng; thus, it proceeds slower than by B because of the smooth 3D shaping (e.g., spherical) of g. On the opposite side, the FSP opening/closing by nB is computationally less demanding than the FP opening/closing by ng. (See [10] for more comparisons.)

All the above definitions of 2D SP, FSP, and FP openings and closings are valid for signals of any dimensionality, simply by using signals f, X, and patterns g, B defined on $\mathbf{R}^m$ or $\mathbf{Z}^m$, $m \geq 1$. For continuous-space signals, we must replace the min/max of all the FP or FSP operations with inf/sup, the finite support of B and g with compact sets, and the discrete patterns nB, ng with the continuous patterns rB, rg. The dimensionality of the pattern B or g

shapes like B) can be measured by $PS_X(p, B)/A(X)$. Finally, the negative-size portion in the pattern spectrum is useful because big impulses at negative sizes illustrate the existence of prominent intruding *gulfs* or *holes* in X. Next we compute analytically the pattern spectra of some simple binary images over $\boldsymbol{R}^2$.

Example 1: Let X be a *disk annulus* of width a with a concentric hole of radius b, like that of Fig. 7. Then, if D is a disk of unit radius and $\delta(r)$ is the Dirac impulse function,

$$PS_X(r, D) = \pi b^2 \delta(r + b) + \pi a(a + 2b)\, \delta\left(r - \frac{a}{2}\right). \tag{24}$$

Example 2: Let Y be a *rectangle* with side lengths a and b, $a \le b$. Then

$$PS_Y(r, D) = 2r(4 - \pi)\left[u(r) - u\left(r - \frac{a}{2}\right)\right] + \left[ab - a^2 + \frac{\pi}{4}a^2\right]\delta\left(r - \frac{a}{2}\right) \tag{25}$$

where $u(r) = \int_{-\infty}^{r} \delta(x)\, dx$ is the unit step function. By contrast, if S is a square (whose one side is parallel to one side of Y) of unit side length,

$$PS_Y(r, S) = ab\delta(r - a). \tag{26}$$

Example 3: Let W be a *regular polygon* with n sides, $n \ge 3$, each of length a. Then its pattern spectra relative to the disk D and to a (unit side length) regular n-gon pattern $T = (1/a)W$ are

$$PS_W(r, D) = 2r\left(n \tan\left(\frac{\pi}{n}\right) - \pi\right) \cdot \left[u(r) - u\left(r - \frac{a}{2\tan\left(\frac{\pi}{n}\right)}\right)\right] + \frac{\pi a^2}{4\tan^2\left(\frac{\pi}{n}\right)}\, \delta\left(r - \frac{a}{2\tan\left(\frac{\pi}{n}\right)}\right)$$

$$PS_W(r, T) = \frac{na^2}{4\tan\left(\frac{\pi}{n}\right)}\, \delta(r - a). \tag{27}$$

If W is inscribed inside a disk of *fixed* radius ρ, then $a = 2\rho \sin(\pi/n)$ and

$$PS_W(r, D) = 2r\left(n \tan\left(\frac{\pi}{n}\right) - \pi\right) \cdot \left[u(r) - u\left(r - \rho\cos\left(\frac{\pi}{n}\right)\right)\right] + \pi\rho^2 \cos^2\left(\frac{\pi}{n}\right) \delta\left(r - \rho\cos\left(\frac{\pi}{n}\right)\right). \tag{28}$$

In the limit as $n \to \infty$, $n \tan(\pi/n) \downarrow \pi$, $\cos(\pi/n) \to 1$, and (28) tends to the pattern spectrum of a disk, i.e., a Dirac impulse at $r = \rho$.

B. Graytone Images (Multilevel Signals)

Our analysis in Section III-A is also valid for sets $X, B \subseteq \boldsymbol{R}^m$ of any dimensionality. In particular, if we let X and B become, respectively, the umbrae of an input multilevel signal and a graytone pattern, then we can extend the pattern spectrum to multilevel signals. Specifically, let $f(x)$, $x \in \boldsymbol{R}^m$, $m = 1, 2, \cdots$, be a nonnegative $m - D$ multilevel signal (e.g., a graytone image if $m = 2$), and let $g(x)$ be any graytone pattern with a *convex umbra* $U(g)$. Then we define the pattern spectrum of f by

$$PS_f(+r, g) = -\frac{dA(f \circ rg)}{dr}, \qquad r \ge 0$$

$$PS_f(-r, g) = \frac{dA(f \bullet rg)}{dr}, \qquad r > 0 \tag{29}$$

where $A(f) = \int_{R^m} f(x)\, dx$ is the finite area under the graph of f.[4] If g is binary and $B \subseteq \boldsymbol{R}^m$ is its compact and convex support, then we can obtain the pattern spectrum of f relative to binary patterns B by replacing the multiscale FP openings $f \circ rg$ and closings $f \bullet rg$ with their FSP counterparts $f \circ rB$ and $f \bullet rB$. For example, Fig. 9 shows a 1D function f and its pattern spectrum with respect to a binary g whose umbra is a semiinfinite rectangle, i.e., the top 1D segment B of the rectangle is the support of g. In Fig. 9, we see that the pattern spectrum of f has impulses at sizes (with respect to B) $r = 1$, 3, and 5 because f contains protruding peaks at these sizes, whereas peaks of size 2 or 4 are not observed. Similarly, f contains many intruding valleys at size 2 which show up as a large impulse in the pattern spectrum at size $r = -2$.

IV. Pattern Spectrum of Discrete-Space Images

The analog pattern spectrum, except for very simple input signals and very simple probing patterns B or g, is very difficult to compute analytically. Thus, in order to efficiently use arbitrary B or g we extend here the pattern spectrum ideas to discrete-space binary and graytone images by using the definition of discrete size introduced in Section II-A.

A. Binary Images

Let $X \subseteq \boldsymbol{Z}^2$ be a finite-extent discrete binary image, and let the discrete binary pattern B be any finite subset of $\boldsymbol{Z}^2$. Recall that the nonnegativity of the pattern spectrum for continuous-space images was guaranteed only if the pattern B was *convex*. However, due to our definition of discrete size, the convexity requirement of B is *not* needed for discrete-space images. To prove this, let F, G, $H \subseteq \boldsymbol{Z}^2$ such that $G = F \oplus H$. Then, $G \circ F = G$ and $Y \circ G \subseteq Y \circ F \subseteq Y \bullet F \subseteq Y \bullet G$ for any $Y \subseteq \boldsymbol{Z}^2$ [47], [7].

[4] Assume that $f \circ rg \ge 0$ for all r such that $f \circ rg \ne -\infty$; this can be achieved by adding a dc-bias to f.

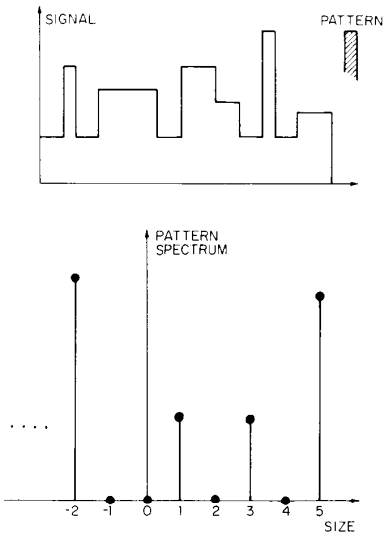

Fig. 9. Pattern spectrum of a 1D multilevel signal.

Hence, (6) implies that for all $n \geq 1$,

$$\cdots \subseteq X \circ (n+1)B \subseteq X \circ nB \cdots \subseteq X \subseteq \cdots$$
$$X \bullet nB \subseteq X \bullet (n+1)B \subseteq \cdots . \tag{30}$$

Thus, $A(X \circ nB)$ can only decrease as n increases where $A(\cdot)$ denotes here finite set cardinality. Since X is finite, there is a positive integer $N = \max\{n: X \ominus nB \neq \varnothing\}$ such that $X \circ nB = \varnothing$ for all $n > N$. Likewise, there is a limit size for successive closings. That is, let $CH(X)$ be the *convex hull* of X, i.e., the intersection of all half planes in $\boldsymbol{Z}^2$ that contain X. For any closed $S \subseteq \boldsymbol{R}^2$ and bounded $G \subseteq \boldsymbol{R}^2$, $S \bullet G \subseteq CH(S)$ [6]. Hence, since $X \subseteq \boldsymbol{Z}^2$ is closed (by being discrete) and $nB \subseteq \boldsymbol{Z}^2$ is bounded (by being finite), we infer that the finite $CH(X)$ includes all terms of the increasing set sequence $X \bullet nB$. Thus $\lim_{n\to\infty}(X \bullet nB) = \mathfrak{L} \subseteq CH(X)$ where

$$\mathfrak{L} = \bigcup_{n \geq 0} X \bullet nB = X \bullet KB. \tag{31}$$

The set limit $\mathfrak{L}$ will be attained for a finite size $n = K$ because X is finite. Obviously, N, K, and $\mathfrak{L}$ depend on both X and B. Fig. 10 shows the different limits sets obtained by using an octagon and a square pattern B, none of which achieves the true convex hull of X.

We define the *pattern spectrum* of X as the nonnegative function

$$PS_X(+n, B) = A[X \circ nB \setminus X \circ (n+1)B], \quad n \geq 0$$
$$PS_X(-n, B) = A[X \bullet nB \setminus X \bullet (n-1)B], \quad n \geq 1 \tag{32}$$

where in (32) $S \setminus Q = \{x \in S: x \notin Q\}$ denotes set difference. Due to (30), $PS_X(n, B) = A(X \circ nB) - A[X \circ (n+1)B]$; hence the discrete pattern spectrum can be obtained via a forward area difference. We will suppress X or B from the general notation of (32) if they are assumed. Obviously, $PS(n) = 0$ for all $n > N$ and all $n < -K$. The B-shapiness of X can be measured by $PS_X(N, B)/A(X)$. As a simple example, Fig. 11 shows a binary image and its pattern spectrum with respect to four patterns of Fig. 4. The shapiness of the image in Fig. 11(a) relative to the line, triangle, square, and rhombus of Fig. 4 is 0.16, 0.98, 0.5, and 0.5, respectively; hence, it is shaped mostly like a triangle.

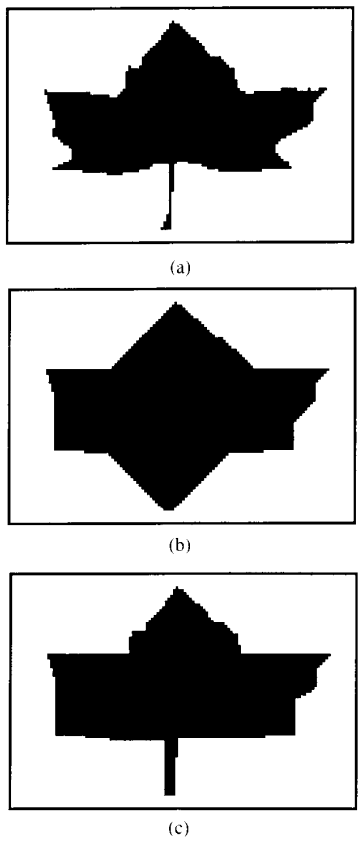

Fig. 10. Approximations $\mathfrak{L}$ to the convex hulls of discrete binary images. (a) Binary image X of 85 × 128 pixels. (b) Set limit $\mathfrak{L}$ with respect to the octagon of Fig. 4 ($K = 8$). (c) $\mathfrak{L}$ with respect to the square of Fig. 4 ($K = 15$).

As an aside, if a finite binary image X is *not connected*, it will be in general equal to the union of its I (disjoint) connected components Y^i. Then $A(X \circ nB = \cup_i Y^i \circ nB) = \Sigma_i A(Y^i \circ nB)$ because $Y^i \cap Y^j = \varnothing \ \forall i \neq j$. Hence, the pattern spectrum of X is the sum

$$PS_X(n, B) = \sum_{i=1}^{I} PS_{Y^i}(n, B) \tag{33}$$

of the pattern spectra of its connected components.

B. Graytone Images (Multilevel Signals)

Let $f(x, y)$, $(x, y) \in \boldsymbol{Z}^2$, be a (nonnegative) *graytone image* function with a finite support. Then we define the *pattern spectrum* of f relative to a discrete graytone pat-

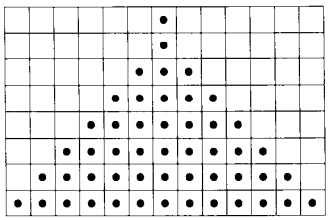

(a)

size n	0	1	2	3	4	5	6	7
$PS(n,\text{line})$	2	4	6	8	10	12	0	8
$PS(n,\text{triangle})$	1	0	0	0	0	0	49	0
$PS(n,\text{square})$	4	4	9	8	25	0	0	0
$PS(n,\text{rhombus})$	5	8	12	25	0	0	0	0

(b)

pattern	av. size	av. roughness
line	3.92	2.65
triangle	5.88	0.14
square	2.92	1.95
rhombus	2.14	1.75

(c)

Fig. 11. (a) A finite 8-connected binary image X. (b) Pattern spectrum of X. (c) Average size and roughness of X.

tern g by the nonnegative function

$$PS_f(+n, g) = A[f \circ ng - f \circ (n+1)g], \quad 0 \le n \le N$$
$$PS_f(-n, g) = A[f \bullet ng - f \bullet (n-1)g], \quad 1 \le n \le K \tag{34}$$

where in (34) $A(f) = \Sigma_{(x,y)} f(x, y)$, and $(a - b)(x) = a(x) - b(x)$ denotes the pointwise algebraic difference between functions $a(x)$ and $b(x)$. N is the maximum (positive) size n such that $f \ominus ng$ is not all $-\infty$; if g is not binary, it is assumed that f has sufficient dc-bias so that $f \circ ng \ge 0\ \forall n \le N$. K is the minimum size n such that $U(f \bullet Kg) = \lim_{n\to\infty} U(f \bullet ng) \subseteq CH[U(f)]$. Obviously, $PS(n) = 0$ for all $n > N$ and all $n < -K$. By contrast to the continuous case (29), convexity of $U(g)$ is *not* needed to guarantee the nonnegativity of (34), because for all $n \ge 1$,

$$\cdots < f \circ (n+1)g \le f \circ ng \cdots \le f \le \cdots$$
$$f \bullet ng \le f \bullet (n+1)g \le \cdots \tag{35}$$

where, for two functions $a(x)$ and $b(x)$, $a \le b$ means that $a(x) \le b(x)$ for all x. Hence, $PS_f(n, g) = A(f \circ ng) - A[f \circ (n+1)g] \ge 0\ \forall n \ge 0$.

We can also define a pattern spectrum of f relative to discrete binary patterns B by replacing $f \circ ng$ and $f \bullet ng$ in (34) and (35) with their FSP counterparts $f \circ nB$ and $f \bullet nB$. In addition, f and g could be 1D or multi-D multilevel signals.

V. Oriented Pattern Spectrum

Fig. 12(a) shows a 2D set X consisting of four circle diagonals spaced by 45°. Its pattern spectrum with respect to a disk [see Fig. 12(b)] conveys no useful information. To enable the pattern spectrum to extract information about the 1D line structures of X that live on a 2D space, we introduce the *oriented pattern spectrum*

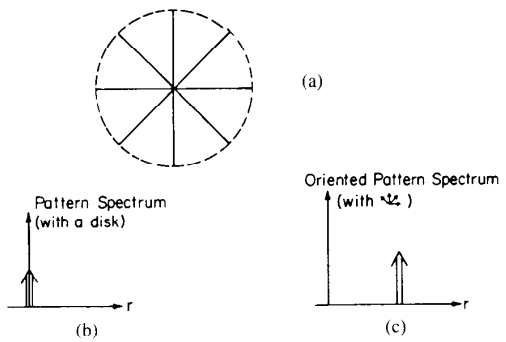

Fig. 12. (a) A binary image $X \subseteq \boldsymbol{R}^2$. (b) Pattern spectrum (nonnegative-size part) of X relative to a disk. (c) Oriented pattern spectrum of X.

$$OPS_X(+r) = -\frac{dA\left(\bigcup_\theta X \circ rL_\theta\right)}{dr}, \quad r \ge 0,$$
$$OPS_X(-r) = \frac{dA\left(\bigcap_\theta X \bullet rL_\theta\right)}{dr}, \quad r > 0 \tag{36}$$

where L_θ is a unit-length *line segment* L passing through the origin of $\boldsymbol{R}^2$ and forming an angle θ with the horizontal. In (36) θ can vary continuously, e.g., $0 \le \theta < 2\pi$, or can assume only a finite number of orientations. For example, for discrete binary images we can choose L as the line pattern of Fig. 4, $\theta \in \{0°, 45°, 90°, 135°\}$, and r becomes the discrete size n. Fig. 12(c) shows the oriented pattern spectrum of Fig. 12(a) [θ assumed only four orientations: 0°, 45°, 90°, 135°], which indicates the existence of major substructure(s) at size equal to the diagonal length.

For 2D graytone image functions $f(x, y)$, we define their oriented pattern spectrum by

$$OPS_f(+r) = -\frac{dA\left[\max_\theta \left\{f \circ rg_\theta(x, y)\right\}\right]}{dr}, \quad r \ge 0,$$
$$OPS_f(-r) = \frac{dA\left[\min_\theta \left\{f \bullet rg_\theta(x, y)\right\}\right]}{dr}, \quad r > 0 \tag{37}$$

where $g_\theta(z)$ is a 1D function oriented at angle θ with compact support and convex umbra. Discrete oriented pattern spectra are obtained by replacing in (36) and (37) the derivatives with finite differences, and rg_θ with ng_θ computed as in (8). The idea of using (for feature extraction) discrete 2D max-of-openings by several 1D sets at different orientations appears in [7]. Areas of oriented openings were used in [46] for texture analysis. 2D max of open-

ings followed by closings by four 1D sets was also investigated in [37] for noise suppression and compared to similar max-of-medians.

VI. Shape-Size Complexity

In the theory of random sets $Y \subseteq \boldsymbol{R}^2$, the *size function* $\Lambda_Y(x) = \sup\{r \geq 0: x \in Y \circ rD\}$ can be viewed for each $x \in Y$ as a random variable representing the size of the set Y measured at point x with respect to a disk D (the measuring "standard") [6], [7]. Keeping B fixed, we define for the finite image $X \subseteq \boldsymbol{Z}^2$ the *discrete random variable*

$$\lambda_X(z) = \max\{n: z \in X \circ nB\}, \qquad z \in X. \quad (38)$$

Assuming stationary random sets, the probability function $p_\lambda(k) = \text{Prob}\{\lambda_X(z) = k\}$ of λ is equal to $PS_X(k, B)/A(X)$, $0 \leq k \leq N$, and hence it is directly related to the pattern spectrum. Now we can treat the size distribution of X from a probabilistic viewpoint. Thus we can define the *average size* $\bar{n}(X/B)$ of X relative to B as the expected value of λ

$$\bar{n}(X/B) = \sum_{n=0}^{N} n p_\lambda(n). \quad (39)$$

Using concepts from information theory, the function

$$H(X/B) = -\sum_{n=0}^{N} p_\lambda(n) \log [p_\lambda(n)] \quad (40)$$

is the average uncertainty (entropy) of the random variable λ. The maximum value of $H(X/B)$ is attained whenever the size histogram is flat. Its minimum value (0) is attained whenever the size histogram contains just an impulse at, say, $n = k$; then X is the union only of maximal (by set inclusion) patterns kB. We define as *roughness* of X relative to nB the number $\log [1/p_\lambda(n)]$, which is a measure of how little the maximal patterns nB that are not covered by unions of larger patterns protrude in X. That is, the larger the normalized area $X \circ nB \setminus X \circ (n+1)B$ (which measures the protrusion of nB) is, the more X consists of protruding patterns nB, and thus the smoother (less rough) X is relative to nB. Then $H(X/B)$ is the *average roughness* of X relative to B; it quantifies the shape-size complexity of X by measuring its boundary roughness averaged over all depths that B reaches. Thus, $H(X/B)$ is maximum ($\log (N+1)$) iff X contains maximal patterns nB at equal area portions in all sizes n, and minimum (zero) iff X is the union of maximal patterns of only one size. For example, the average size and roughness of the image in Fig. 11(a) relative to various patterns are tabulated in Fig. 11(c).

If X is the union of (disjoint) connected components Y^i, $i = 1, \cdots, I$, let p_i be the size probability function of each Y^i relative to B. From (33), we have $p_\lambda(k) = [\Sigma_i A(Y^i) p_i(k)]/A(X)$ for $k \geq 0$. Then, due to the convexity of the entropy function

$$H(X/B) \geq \frac{1}{A(X)} \cdot \sum_{i=1}^{I} A(Y^i) H(Y^i/B), \quad (41)$$

which implies that the shape-size complexity of X is never smaller than the area-weighted average of the complexities of its connected components.

In the estimation of the average roughness we can incorporate the negative-size portion of the pattern spectrum by extrapolating λ and defining it on each point $z \in \mathcal{L} \setminus X$ as $\lambda_X(z) = -n$ iff $z \in X \bullet nB \setminus X \bullet (n-1)B$; then, in (40) we must also replace $p_\lambda(n)$ with $PS_X(n, B)/A(\mathcal{L})$ and the lower summation limit $n = 0$ with $n = -K$. This new definition of roughness will also take into account the complexity of the *local background*, $\mathcal{L} \setminus X$, of X inside $CH(X)$.

We define the average size and roughness of a graytone image f based on its pattern spectrum exactly as for binary images. Thus, the *average roughness* of f relative to a graytone pattern g is

$$H(f/g) = -\sum_{n=0}^{N} q(n) \log q(n) \quad (42)$$

where $q(n) = PS_f(n, g)/A(f)$. This number $H(f/g)$ quantifies the shape-size complexity of f by measuring its surface roughness (due to its peak distribution) averaged over all depths that g reaches. We can also *normalize* $H(f/g)$ by dividing it with its maximum value, i.e., $\log (N+1)$. For example, Fig. 13 shows two texture graytone images f_1 (texture 1) and f_2 (texture 2). Relative to the octagon of Fig. 4, the normalized average roughnesses of f_1, f_2 are, respectively, 0.54 and 0.63; similarly, relative to a paraboloid graytone pattern g of the same support as the octagon ($g(x, y) = 5 - x^2 - y^2$, $0 \leq x^2 + y^2 \leq 5$), the $H(f_i/g)/\log (N_i + 1)$ were 0.80 and 0.66 for $i = 1, 2$. If we wish $H(f/g)$ to reflect the complexity of f due to both its peaks and valleys, then we could replace in (42) $n = 0$ with $n = -K$ and set $q(n) = PS_f(n, g)/A(f \bullet Kg)$; in this case, normalizing the new $H(f/g)$ requires dividing it with $\log (N + K + 1)$. Finally, the complexity measure $H(f/g)$ can be extended to continuous-space images by replacing discrete pattern spectra with their continuous versions and summation over n with integration over the continuous size r.

VII. Skeleton Transforms for Binary Images

A. Morphological Skeleton Transform

Let $X \subseteq \boldsymbol{Z}^2$ represent a finite-extent discrete binary image and let $B \subseteq \boldsymbol{Z}^2$ be a fixed (finite) binary pattern with $(0, 0) \in B$. It was shown in [26], [38], [33], [7], [34] that successive erosions and openings yield the *skeleton components*

$$S_n = (X \ominus nB) \setminus [(X \ominus nB) \circ B], \qquad n = 0, 1, \cdots, N, \quad (43)$$

of X with respect to B where $N = \max\{n \geq 0: X \ominus nB \neq \varnothing\}$. Each S_n is a subset of X indexed by the discrete size parameter n and depends both on X and B. The union of all S_n is the *morphological skeleton* $SK(X)$ of X. The information in *all* the S_n can be represented compactly by the *skeleton function* whose support is equal to $SK(X)$

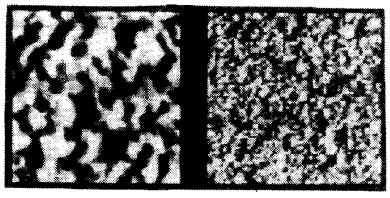

texture 1 texture 2

Fig. 13. Two graytone 64 × 64-pixel images of textures.

and whose value at the skeleton pixel z is n if $z \in S_n$. Alternatively, the same information is conveyed by the *morphological skeleton transform* of X which we define as the finite set-valued sequence

$$ST(X) = (S_0, S_1, S_2, \cdots, S_N). \tag{44}$$

From $ST(X)$ we can reconstruct X, i.e.,

$$X \circ kB = \bigcup_{k \le n \le N} S_n \oplus nB, \qquad 0 \le k \le N. \tag{45}$$

Thus, if $k = 0$ (i.e., if we use all the skeleton subsets), $X \circ kB = X$ and we have *exact reconstruction*. If $1 \le k \le N$, we obtain a *partial reconstruction*, i.e., the opening (smoothed version) of X by kB [34]. The larger the k, the larger the degree of smoothing.

Among similar approaches to shape smoothing via the skeleton, Miller [38] called the S_n a "shrink-expand series representation" and observed that elimination of some low-index S_n provides some boundary smoothing. Duda and Hart [39] noticed that suppressing the small-amplitude pixels in the skeleton function provides some shape smoothing. Ho and Dyer [40] improved this procedure by first normalizing the skeleton function according to the relative prominence of each skeleton point and then by eliminating the minor branches of the modified skeleton function. Dill *et al.* [41] investigated the skeletonization of binary images whose boundary curvature functions were filtered by linear low-pass filters of varying spatial resolution. Similarly, Pizer *et al.* [42] explore skeletonization of binary images at multiple scales provided either by B spline smoothing of the boundary or by Gaussian smoothing of the binary image function. Note that in [41], [42] the image is skeletonized at each scale, whereas in our approach and in [38]–[40] it is skeletonized only once. Moreover in [38]–[42] the relationships between shape smoothing and skeleton information were only *qualitative*. By contrast, in our approach, the shape smoothing can be *quantified* precisely via openings.

If B is a symmetric (i.e., $B = \check{B}$) disk-like pattern like the square or rhombus of Fig. 4, then $SK(X)$ is the well-known (discrete) medial axis of X. If B is an asymmetric or a 1D set, then $SK(X)$ does not look any more like a symmetry axis, but it highlights various other features of the shape X [34].

Both the skeleton decomposition (for all n) algorithm (43) and the reconstruction (for one k) algorithm (45) require $O(N^2)$ erosions/dilations by B. Faster algorithms, requiring $O(N)$ erosions/dilations, can be found in [34]. Such a faster reconstruction algorithm can be written analytically as

$$X \circ kB = \left[\left((S_N \oplus B) \cup S_{N-1}\right) \oplus B \cdots \cup S_k\right] \oplus kB \tag{46}$$

for $0 \le k \le N$.

B. Reduced Skeleton Transform (RST)

Independently of B, all $ST(X)$ can reconstruct exactly X, and $SK(X)$ looks like an "axis." At the expense of producing a skeleton that may not look like a skeletal axis, we define the *minimal skeleton transform* to be a sequence of indexed skeleton components that are subsets of the original S_n but without redundancy, i.e., capable for exact reconstruction but such that removal of just one point would violate the exact (or partial) reconstruction controlled by (45). Fast searching algorithms were developed in [34] to find a minimal skeleton. In this paper, we provide an analytic formula for a "reduced" skeleton transform (RST). The RST may not always be able to subtract *all* the redundancy in the skeleton (as the minimal skeleton does). It may, however, eliminate *some* redundancy, since it never contains more points than the original skeleton. Our reason for introducing the RST is that it is fully compatible with the pattern spectrum as explained later. The nth *reduced skeleton component* of X (with respect to B) is defined as the set

$$R_n = (X \ominus nB) \setminus \left[\left[(X \ominus nB) \circ B\right] \bullet nB\right], \qquad 0 \le n \le N. \tag{47}$$

Since, for any set S and G, $(S \ominus G) \bullet G = S \ominus G$ [7], we have $(X \ominus nB) \circ B \subseteq [(X \ominus nB) \circ B] \bullet nB \subseteq (X \ominus nB) \bullet nB = X \ominus nB$. Thus,

$$R_n \subseteq S_n \subseteq X \ominus nB, \qquad 0 \le n \le N,$$

and hence, R_n eliminates some redundancy from S_n. Note also that $R_0 = S_0$ and $R_N = S_N = X \ominus NB$. The algorithm (47) can be implemented efficiently by recursively obtaining the successive erosions as $X \ominus nB = [X \ominus (n-1)B] \ominus B$, $n = 1, \cdots, N$; then (47) requires $N^2 + N + 1$ erosions/dilations by B of an image array initially holding X.

The union of all R_n is the *reduced skeleton*, $RS(X)$, of X. The *reduced skeleton transform* (RST) of X with respect to B is the finite set-valued sequence

$$\text{RST}(X) = (R_0, R_1, R_2, \cdots, R_N). \tag{48}$$

From RST (X) we can reconstruct X. That is, for $0 \le k \le N$, let $T_k = (X \ominus kB) \circ B$. Then,

$$\begin{aligned}(T_k \bullet kB) \oplus kB &= (T_k \oplus kB) \circ kB = T_k \oplus kB \\ &= \left(\left((X \ominus kB) \ominus B\right) \oplus B\right) \oplus kB \\ &= X \circ (k+1)B.\end{aligned}$$

This result together with the fact that $X \ominus kB = R_k \cup (T_k \bullet kB)$ imply

$$X \circ kB = (R_k \oplus kB) \cup [X \circ (k+1)B], \quad 0 \le k \le N. \tag{49}$$

Since also $R_N = X \ominus NB$, it follows that

$$X \circ kB = \bigcup_{k \le n \le N} R_n \oplus nB, \quad 0 \le k \le N. \tag{50}$$

The reconstruction (50) requires (for each k) $O(N^2)$ dilations by B. Since dilation commutes with union, (50) is equivalent to the faster algorithm below

$$X \circ kB = [((R_N \oplus B) \cup R_{N-1}) \oplus B \cdots \cup R_k] \oplus kB. \tag{51}$$

The algorithm (51) requires N dilations by B.

The original and reduced skeletons (with respect to the octagon of Fig. 4) of the binary leaf image of Fig. 10(a) are identical and both contain 303 pixels. However, this is not always the case because we have found cases where the RST has fewer points than the original skeleton. For example, the original skeleton of Fig. 10(a) with respect to the square of Fig. 4 has 194 pixels, whereas the reduced skeleton has 182 pixels. In our experiments, we found that the RST could eliminate about 0–6 percent of the original skeleton points. (The minimal skeleton has achieved in some cases elimination of about 50 percent of original skeleton points [34].) We also observed that the ability of RST to subtract redundancy from the original skeleton increases with the size of the image.

C. Relations Between RST and Pattern Spectrum

Let $PS(n)$ be the pattern spectrum of X relative to B. Observe from (45) that $S_n = \varnothing$ implies $X \circ nB = X \circ (n+1)B$, and hence,

$$S_n = \varnothing \Rightarrow PS(n) = 0, \quad n \ge 0. \tag{52}$$

The converse of (52) is not generally true. However, a closer relationship exists between pattern spectrum and RST. That is, consider the sets

$$D_k = (X \circ kB) \setminus [X \circ (k+1)B], \quad 0 \le k \le N. \tag{53}$$

Then, for $0 \le n \le N-1$,

$$\begin{aligned} R_n = \varnothing &\Rightarrow X \ominus nB = [(X \ominus nB) \circ B] \bullet nB \\ &\Rightarrow X \circ nB = X \circ (n+1)B \\ &\Rightarrow D_n = \varnothing. \end{aligned}$$

Conversely, for $0 \le n \le N-1$,

$$\begin{aligned} D_n = \varnothing &\Rightarrow X \circ nB = X \circ (n+1)B \\ &\Rightarrow (X \ominus nB) \oplus nB = [(X \ominus nB) \circ B] \oplus nB \\ &\Rightarrow X \ominus nB = [(X \ominus nB) \circ B] \bullet nB \\ &\Rightarrow R_n = \varnothing. \end{aligned}$$

Thus, for $0 \le n \le N-1$,

$$R_n = \varnothing \Leftrightarrow D_n = \varnothing \Leftrightarrow PS(n) = 0, \tag{54}$$

which provides the major link between pattern spectrum, RST, and multiscale openings. Note that $R_N = D_N \ne \varnothing$.

From (50), (54), and (30) it also follows that for $1 \le k \le N$,

$$\begin{aligned} X = X \circ kB &\Leftrightarrow PS(n) = 0 \quad 0 \le n < k \\ &\Leftrightarrow R_n = \varnothing \quad 0 \le n < k. \end{aligned} \tag{55}$$

Thus, X is smooth to a degree k relative to B (i.e., $X = X \circ kB$) if and only if its first k pattern spectrum samples are zero, or equivalently, if and only if its first k reduced skeleton components are empty. Hence, the sets R_n behave as shape-size components of X.

To relate RST with the pattern spectrum at *negative sizes*, we extrapolate the RST by skeletonization of the background X^c of X. Thus, we define as the *extended reduced skeleton transform* (ERST) the finite set sequence

$$\text{ERST}(X) = (R_{-K}, R_{-K+1}, \cdots, R_{-1}, R_0, R_1, \cdots, R_N) \tag{56}$$

where for $0 \le n \le K-1$ the sets

$$R_{-n-1} = [[(X \oplus nB) \bullet B] \circ nB] \setminus (X \oplus nB) \tag{57}$$

are reduced skeleton components of X^c, and $K = \min\{k \ge 0: X \bullet nB = X \bullet kB \ \forall n > k\}$. Thus, $R_{-n} = \varnothing \ \forall n > K$. If we define

$$D_{-n} = (X \bullet nB) \setminus [X \bullet (n-1)B], \quad 1 \le n \le K \tag{58}$$

by working as for (54) it can be shown that, for $1 \le n \le K$

$$R_{-n} = \varnothing \Leftrightarrow D_{-n} = \varnothing \Leftrightarrow PS(-n) = 0. \tag{59}$$

Therefore, for $1 \le k \le K$,

$$\begin{aligned} X = X \bullet kB &\Leftrightarrow R_{-n} = \varnothing \quad 1 \le n \le k \\ &\Leftrightarrow PS(-n) = 0 \quad 1 \le n \le k. \end{aligned} \tag{60}$$

VIII. Skeleton Transforms for Graytone Images

Let $f(x, y)$, $(x, y) \in \mathbf{Z}^2$, represent a finite-support discrete graytone image and let $g(x, y)$ be a fixed discrete graytone pattern with $g(0, 0) \ge 0$. The *skeleton components* of f with respect to g are the functions

$$s_n = (f \ominus ng) - [(f \ominus ng) \circ g], \quad 0 \le n \le N \tag{61}$$

where $N = \max\{n: f \ominus ng \ne -\infty\}$. (The pointwise sum of all s_n could serve as a morphological skeleton of f.) We call as *morphological skeleton transform* of f with respect to g the finite function-valued sequence

$$ST(f) = (s_0, s_1, s_2, \cdots, s_N). \tag{62}$$

From $ST(f)$ we can reconstruct f:

$$f \circ kg = \left[((s_N \oplus g) + s_{N-1}) \oplus g \cdots + s_k\right] \oplus kg \tag{63}$$

for $0 \le k \le N$. Thus, if $k = 0$, $f \circ kg = f$ and we have *exact reconstruction*. If $1 \le k \le N$, we obtain a *partial reconstruction*, i.e., the opening (smoothed version) of f by kg. The larger the k, the larger the degree of smoothing.

To implement (61) and (63) when g is *not* binary, f should have sufficient dc-bias so that $f \ominus ng \ge 0$ $\forall n \le N$. In addition, pixels outside the support of any added or resulting function are set equal to $-\infty$, and $p \pm (-\infty)$ is set equal to p for any $p \ge -\infty$. For example, Fig. 14 shows an 8×8-pixel graytone image h to be skeletonized by a graytone pattern g, defined on $\mathbf{Z}^2$ as $g(x, y) = 2 - (x^2 + y^2)$ for $0 \le x^2 + y^2 \le 2$ and $g(x, y) = -\infty$ elsewhere. Assuming that h is nonnegative, we add to all the pixels in the support of h (i.e., pixels (x, y) with $h(x, y) \ne 0$) a dc-bias $= 3$ and thus create another image f, such that $f \ominus ng \ge 0$ $\forall n \le N = 3$; the four skeleton components of f are shown in Fig. 14. To avoid the above implementation issues one could alternatively use a *binary* g. In this latter case, if B represents the support of g, then $f \ominus g$ and $f \oplus g$ become, respectively, the moving local minimum and maximum of f inside the window B; further, pixels not belonging to the support of f or its skeleton components can be assigned the value "0" because 0 acts as a neutral element for the local min/max operations. Then the skeleton transform of f with respect to B is identical to the gray medial axis transform developed in [28]. It is generally possible to find patterns g and B such that the skeleton transform of an image with respect to g has fewer points or a more desired shape than the skeleton with respect to B, and vice-versa. However, a systematic or optimum (according to some criterion) choice of g or B still remains an open issue.

The nth *reduced skeleton component* of f (with respect to g) is the function

$$r_n = (f \ominus ng) - \left[\left[(f \ominus ng) \circ g\right] \bullet ng\right], \qquad 0 \le n \le N. \tag{64}$$

Since [10], for any functions h and a, $(h \ominus a) \bullet a = h \ominus a$, we have $(f \ominus ng) \circ g \le [(f \ominus ng) \circ g] \bullet ng \le (f \ominus ng) \bullet ng = f \ominus ng$. Thus,

$$r_n \le s_n \le f \ominus ng, \qquad 0 \le n \le N,$$

and hence, r_n eliminates some redundancy from s_n. Note also that $r_0 = s_0$ and $r_N = s_N = f \ominus Ng$. The *reduced skeleton transform* (RST) of f is the finite function sequence

$$\mathrm{RST}(f) = (r_0, r_1, r_2, \cdots, r_N). \tag{65}$$

From RST (f) we can reconstruct f, i.e., for $0 \le k \le N$,

$$f \circ kg = \left[\left[\left[(r_N \oplus g) \bullet (N - 1)g\right] + r_{N-1}\right] \cdots \oplus g \bullet kg + r_k\right] \oplus kg. \tag{66}$$

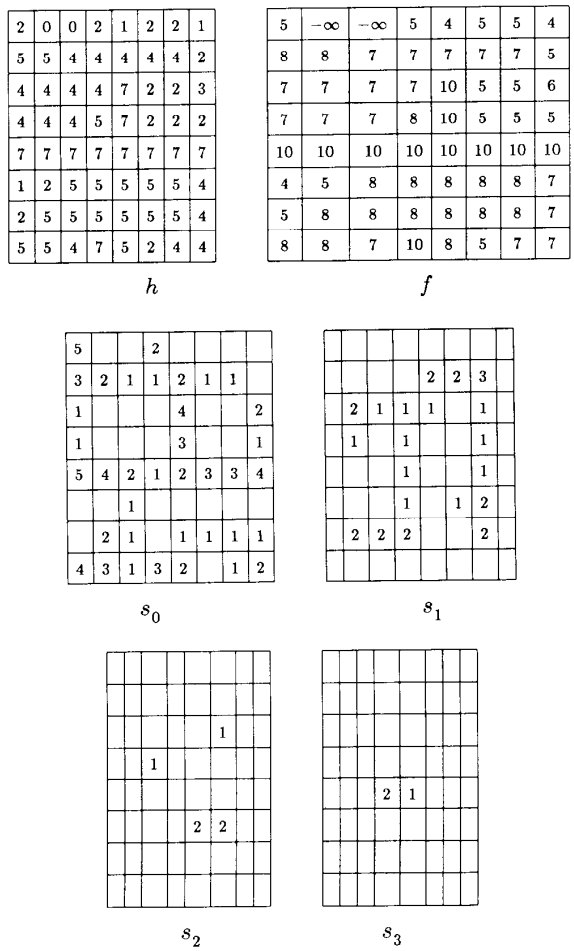

Fig. 14. Skeleton transform for graytone images via *FP* filtering.

In Fig. 14 the original skeleton transform contains the same points as the RST. However, in images of larger size we observed some elimination of original skeleton points by using the RST. For example, Table I shows the number of points in the supports of the original and reduced skeleton components of the graytone image "texture 2" of Fig. 13 with respect to the square of Fig. 4. The total number of points in the original skeleton transform was 5047, whereas the RST had 4983 points.

From (61) it follows that

$$s_n \equiv -\infty \Rightarrow PS_f(n, g) = 0 \tag{67}$$

where, for a function $a(x)$, $a \equiv -\infty$ means that $a(x) = -\infty$ $\forall x$, or equivalently that the number of points in its support is zero. For example, in Table I observe that $PS(7) = 0$ and $s_7 \equiv -\infty$. The converse of (67) is generally true *only if* we use the RST (f). Thus, let the *extended reduced skeleton transform* of f be the finite function sequence

$$\mathrm{ERST}(f) = (r_{-K}, r_{-K+1}, \cdots, r_{-1}, r_0, r_1, \cdots, r_N), \tag{68}$$

TABLE I
PATTERN SPECTRUM, SKELETON TRANSFORM, AND RST OF THE "TEXTURE 2" IMAGE OF FIG. 13[a]

size n	$PS(n)$	$\#(s_n)$	$\#(r_n)$
0	204047	2789	2789
1	115067	1175	1155
2	72569	608	574
3	36439	278	271
4	23497	122	119
5	15564	48	48
6	11019	21	21
7	0	0	0
8	4788	6	6

[a] pattern B = square of Fig. 4; $N = 8$; $\#(f)$ denotes the number of pixels in $\mathrm{Spt}(f)$.

where, for $0 \le n \le K-1$, the functions

$$r_{-n-1} = \left[\left[(f \oplus ng) \bullet g\right] \circ ng\right] - (f \oplus ng) \quad (69)$$

are reduced skeleton components of $(-f)(x, y) = -f(x, y)$, and $K = \min\{k: f \bullet ng = f \bullet kg \ \forall n > k\}$. Now consider the functions

$$d_n = (f \circ ng) - \left[f \circ (n+1)g\right], \qquad 0 \le n \le N.$$
$$d_{-n} = (f \bullet ng) - \left[f \bullet (n-1)g\right], \qquad 1 \le n \le K. \quad (70)$$

Then, if $PS(n)$ is the pattern spectrum of f relative to g, it can be shown that, for $-K \le n \le N$,

$$r_n \equiv -\infty \Leftrightarrow d_n \equiv -\infty \Leftrightarrow PS(n) = 0. \quad (71)$$

From (66), (71), and (35) it also follows that, for $1 \le k \le N$,

$$f = f \circ kg \Leftrightarrow PS(n) = 0 \qquad 0 \le n < k$$
$$\Leftrightarrow r_n \equiv -\infty \qquad 0 \le n < k. \quad (72)$$

Thus, f is smooth with respect to (i.e., does not contain) peaks of size k relative to g if and only if its first k pattern spectrum samples are zero, or equivalently, if and only if its first k reduced skeleton components vanish. Likewise for the relationships among the valleys of f, its pattern spectrum values at negative sizes, and the skeleton components of $-f$. Hence, the functions r_n behave as multiscale shape-size components of f.

IX. CONCLUSIONS

This paper focused on the developments of 1) discrete and continuous multiscale nonlinear smoothing filters based on morphological openings or closings, 2) a shape-size descriptor, the pattern spectrum, based on the area functions of openings or closings at successive scales, 3) an oriented version of pattern spectrum, 4) a shape-size complexity measure as the entropy of a size random variable whose probability function is the pattern spectrum, 5) a reduced skeleton transform for multiscale representation of discrete images based on morphological filtering, and 6) interrelationships among the multiscale filters, the pattern spectrum, and the skeleton transform.

The multiscale openings and closings are useful smoothing filters because they preserve the shape and location of vertical abrupt signal discontinuities (e.g., edges); further, the definition of scale in the openings is identical to the spatial size of geometrical objects. Both of these properties are not shared by multiscale low-pass linear filters; hence, openings/closings could complement and enrich multiscale signal analysis (classically based on linear smoothing). It is also interesting to note that many linear (e.g., averager, Gaussian) and nonlinear (e.g., opening/closing, median) smoothing filters can be represented exactly via erosions or dilations [10]–[12], [14], [36]. The pattern spectrum enriches the usefulness of multiscale openings because large impulses in the pattern spectrum indicate the existence of major (protruding or intruding), substructures in a signal at that scale, and hence provide the critical scales in a multiscale signal analysis. Further, the pattern spectrum quantifies many other aspects of the shape-size content of the signal, e.g., the complexity of the image boundary or surface (due to its peak/valley size distribution) can be measured from the pattern spectrum. The (original or reduced) skeleton transform can serve as a compact representation in multiscale image analysis because 1) the skeleton components are sparse images and hence can encode the image efficiently, and 2) the partially reconstructed images from the inverse transform on subsequences of skeleton components are exactly the openings of the image at a scale determined by the number of eliminated skeleton components. In addition, due to the strong links between the morphological (original or reduced) skeleton transform, the multiscale openings, and the pattern spectrum, the latter two appear to be powerful tools to study multiscale representations that are based on skeletonization. Finally, we outline how the ideas in this paper could be used for multiscale feature extraction.

1) Edge/Line Enhancement: At a *single* scale, the difference $f - (f \ominus W)$ where W is a small symmetric structuring set, enhances the edges of the signal or image f [29], [38], [7], [36]. In [43], this scheme was improved by first smoothing f with a linear blur, which made it a robust edge detector. This linear blur was replaced by an alpha-trimmed mean filter in [44]. For a *multiple scale* edge enhancement we propose the following simple process:

$$(f \circ ng) - \left[(f \circ ng) \ominus W\right] \quad (73)$$

where the opening by ng performs a multiscale smoothing before the edges are enhanced. The shape of g controls the shape of smoothing, and the size n controls the scale. Preliminary experiments at the Harvard Robotics Lab in-

dicate that (73) is promising for multiscale edge/line enhancement and very simple to implement. If the features to be enhanced are 1D line structures, then the opening by ng will eliminate them if g has a 2D support; to avoid this, one could use a max-of-openings (or a min-of-closings) by g with 1D support oriented at different angles.

2) Edge Detection: In [1], the edges $E(f)$ of an image f were defined as the zero-crossing points of the signal $\nabla^2(G_\sigma * f)$ where G_σ is a Gaussian of standard deviation σ and $*$ denotes linear convolution. In view of the advantages of the openings for preserving edges while smoothing, we propose the following edge detection process:

$$E(f) = \left\{(x, y): [\nabla^2(f \circ ng)](x, y) = 0\right\}. \quad (74)$$

A nice property of the $\nabla^2(G_\sigma * f)$ edge detector is that additional edges are not introduced at coarser scales. Chen and Yan [15] have shown that the zero-crossings of the 1D boundary curvature function of the successive openings of a compact continuous binary image by disks of radii r do not increase at coarser scales (larger r). It remains to be seen whether this important result is also true for 2D continuous graytone images and/or for discrete graytone images whose edges are defined by (74) using a discrete approximation to ∇^2. In both schemes (73) and (74), the pattern spectrum (or its oriented version) could also be used to find the critical scales for feature detection.

Acknowledgment

The author wishes to thank Dr. F.-K. Sun of TASC for many encouraging and helpful discussions on the use of pattern spectra.

References

[1] D. Marr and E. Hildreth, "Theory of edge detection," *Proc. Rev. Soc. Lond., B*, vol. 207, pp. 187–217, 1980.

[2] A. Witkin, "Scale-space filtering," in *Proc. IJCAI*, Carlsrue, W. Germany, 1983, pp. 1019–1022.

[3] A. Yuille and T. Poggio, "Scaling theorems for zero crossings," *IEEE Trans. Pattern. Anal. Machine Intell.*, vol. PAMI-8, pp. 15–25, Jan. 1986.

[4] P. J. Burt and E. H. Adelson, "The Laplacian pyramid as a compact image code," *IEEE Trans. Commun.*, vol. COM-31, pp. 532–540, Apr. 1983.

[5] A. Rosenfeld, Ed., *Multiresolution Image Processing and Analysis*. New York: Springer Verlag, 1984.

[6] G. Matheron, *Random Sets and Integral Geometry*. New York: Wiley, 1975.

[7] J. Serra, *Image Analysis and Mathematical Morphology*. New York: Academic, 1982.

[8] S. R. Sternberg, "Grayscale morphology," *Comput. Vision, Graph, Image Processing*, vol. 35, pp. 333–355, 1986.

[9] R. M. Haralick, S. R. Sternberg, and X. Zhuang, "Image analysis using mathematical morphology," *IEEE Trans. Pattern Anal. Machine Intell.*, vol. PAMI-9, pp. 523–550, July 1987.

[10] P. Maragos and R. W. Schafer, "Morphological filters—Part I: Their set-theoretic analysis and relations to linear shift-invariant filters," *IEEE Trans. Acoust., Speech, Signal Processing*, vol. ASSP-35, pp. 1153–1169, Aug. 1987.

[11] ——, "Morphological filters—Part II: Their relations to median, order-statistic, and stack filters," *IEEE Trans. Acoust., Speech, Signal Processing*, vol. ASSP-35, pp. 1170–1184, Aug. 1987.

[12] P. Maragos, "A unified theory of translation-invariant systems with applications to morphological analysis and coding of images," Ph.D. dissertation, School of Elec. Eng., Georgia Inst. Technol., Atlanta, GA, July 1985.

[13] ——, "Pattern spectrum of images and morphological shape-size complexity," in *Proc. IEEE ICASSP'87*, Dallas, TX, Apr. 1987, pp. 241–244.

[14] ——, "Morphology-based multidimensional signal processing," in *Proc. 21st Annu. Conf. Inform. Sci. Syst.*, Johns Hopkins Univ., Baltimore, MD, Mar. 1987, pp. 513–518.

[15] M. Chen and P. Yan, "A multiscaling approach based on morphological filtering," submitted to *IEEE Trans. Pattern Anal. Machine Intell.*

[16] R. M. Haralick, C. Lin, J. S. J. Lee, and X. Zhuang, "Multiresolution morphology," in *Proc. 1st ICCV*, London, England, June 1987.

[17] H. Blum, "A transformation for extracting new descriptions of shape," in *Models for the Perception of Speech and Visual Forms*, W. Wathen-Dunn, Ed. Cambridge, MA: M.I.T. Press, 1967.

[18] ——, "Biological shape and visual senses (Part I)," *J. Theor. Biol.*, vol. 38, pp. 205–287, 1973.

[19] H. Blum and R. N. Nagel, "Shape description using weighted symmetric axis features," *Pattern Recogn.*, vol. 10, pp. 167–180, 1978.

[20] L. R. Nackman and S. M. Pizer, "Three-dimensional shape description using the symmetric axis transform I: Theory," *IEEE Trans. Pattern Anal. Machine Intell.*, vol. PAMI-7, pp. 187–202, Mar. 1985.

[21] T. Pavlidis, "Algorithms for shape analysis of contours and waveforms," *IEEE Trans. Pattern. Anal. Machine Intell.*, vol. PAMI-2, pp. 301–312, Jul. 1980.

[22] M. Brady and H. Asada, "Smoothed local symmetries and their implementation," M.I.T. Artif. Intell. Lab, A.I. Memo 757, Feb. 1984.

[23] A. Rosenfeld, "Axial representations of shape," *Comput. Vision Graph. Image Processing*, vol. 33, pp. 156–173, 1986.

[24] A. Rosenfeld and J. L. Pfaltz, "Sequential operations in digital picture processing," *J. Assoc. Comp. Mach.*, vol. 13, pp. 471–494, Oct. 1966.

[25] J. L. Pfaltz and A. Rosenfeld, "Computer representations of planar regions by their skeletons," *Commun. Assoc. Comp. Mach.*, vol. 10, pp. 119–122, Feb. 1967.

[26] J. C. Mott-Smith, "Medial axis transformations," in *Picture Processing and Psychopictorics*, B. S. Lipkin and A. Rosenfeld, Eds. New York: Academic, 1970.

[27] Y. Nakagawa and A. Rosenfeld, "A note on the use of local min and max operations in digital picture processing," *IEEE Trans. Syst., Man, Cybern.*, vol. SMC-8, pp. 632–635, Aug. 1978.

[28] S. Peleg and A. Rosenfeld, "A min-max medial axis transformation," *IEEE Trans. Pattern. Anal. Machine Intell.*, vol. PAMI-3, pp. 208–210, Mar. 1981.

[29] V. Goetcherian, "From binary to grey tone image processing using fuzzy logic concepts," *Pattern Recogn.*, vol. 12, pp. 7–15, 1980.

[30] K. Preston, Jr., M. J. B. Duff, S. Levialdi, P. E. Norgren, and J-I. Toriwaki, "Basics of cellular logic with some applications in medical image processing," *Proc. IEEE*, vol. 67, pp. 826–856, May 1979.

[31] K. Preston, Jr., "Ξ-Filters," *IEEE Trans. Acoust., Speech, Signal Processing*, vol. ASSP-31, pp. 861–876, Aug. 1983.

[32] C. Arcelli, L. P. Cordella, and S. Levialdi, "From local maxima to connected skeletons," *IEEE Trans. Pattern Anal. Machine Intell.*, vol. PAMI-3, pp. 134–143, Mar. 1981.

[33] C. Lantuejoul, "Skeletonization in quantitative metallography," in *Issues of Digital Image Processing*, R. M. Haralick and J. C. Simon, Eds. Groningen, The Netherlands: Sijthoff and Noordhoff, 1980.

[34] P. Maragos and R. W. Schafer, "Morphological skeleton representation and coding of binary images," *IEEE Trans. Acoust., Speech, Signal Processing*, vol. ASSP-34, pp. 1228–1244, Oct. 1986.

[35] H. Hadwiger, *Vorlesungen über Inhalt, Oberfläche, und Isoperimetrie*. Berlin: Springer Verlag, 1957.

[36] P. Maragos, "Tutorial on advances in morphological image processing and analysis," *Opt. Eng.*, vol. 26, pp. 623–632, July 1987.

[37] R. L. Stevenson and G. R. Arce, "Morphological filters: Statistics and further syntactic properties," *IEEE Trans. Circuit Syst.*, vol. CAS-34, pp. 1292–1305, Nov. 1987.

[38] P. E. Miller, "An investigation of Boolean image neighborhood transformations," Ph.D. dissertation, Ohio State Univ., 1978.

[39] R. O. Duda and P. E. Hart, *Pattern Classification and Scene Analysis*. New York: Wiley, 1973.

[40] S.-B. Ho and C. R. Dyer, "Shape smoothing using medial axis properties," *IEEE Trans. Pattern. Anal. Machine Intell.*, vol. PAMI-8, pp. 512-520, July 1986.

[41] A. R. Dill, M. D. Levine, and P. B. Noble, "Multiple resolution skeletons," *IEEE Trans. Pattern. Anal. Machine Intell.*, vol. PAMI-9, pp. 495-504, July 1987.

[42] S. M. Pizer, W. R. Oliver, and S. H. Bloomberg, "Hierarchical shape description via the multiresolution symmetric axis transform," *IEEE Trans. Pattern. Anal. Machine Intell.*, vol. PAMI-8, pp. 505-511, July 1987.

[43] J. S. J. Lee, R. M. Haralick, and L. G. Shapiro, "Morphologic edge detection," *IEEE Trans. Rob. Autom.*, vol. RA-3, pp. 142-156, Apr. 1987.

[44] R. J. Feehs and G. R. Arce, "Multidimensional morphological edge detection," in *Visual Communications and Image Processing II*, T. R. Hsing, Ed. *Proc. SPIE* 845, pp. 285-292, 1987.

[45] F. Meyer, Empiricism or idealism" in *Pattern Recognition in Practice*, E. S. Gelsema and L. N. Kanal, Eds. Amsterdam, The Netherlands: North-Holland, 1980.

[46] M. Werman and S. Peleg, "Min-max operators in texture analysis," *IEEE Trans. Pattern Anal. Machine Intell.*, vol. PAMI-7, pp. 730-733, Nov. 1985.

[47] G. Matheron, *Éléments Pour Une Théorie Des Milieux Poreux*. Paris: Masson et Cie, 1967.

Petros Maragos (S'81-M'85) was born in Kalymnos, Greece, on November 4, 1957. He received the Diploma degree in electrical engineering from the National Technical University of Athens, Greece, in 1980, and the M.S.E.E. and Ph.D. degrees from the Georgia Institute of Technology, Atlanta, in 1982 and 1985, respectively.

From 1980 to 1985 he was a Research Assistant at the Digital Signal Processing Lab of the Electrical Engineering School at Georgia Tech. Since August 1985 he has been an Assistant Professor of Electrical Engineering in the Division of Applied Sciences at Harvard University, Cambridge. His current research interests include signal and image processing, computer vision, and pattern recognition.

Dr. Maragos received a National Science Foundation Presidential Young Investigator Award in 1987.